Supporting Information

Colloid synthesis of hexagonal $CuFe(S_xSe_{1-x})_2$ nanoplates with exposed highly-active (220) facets for boosting overall water splitting

Shoushuang Huang, [a] Xiansheng Cong, [a] Tong Ye, [a] Libin Liu, [a] Kaimei Peng,*[b] Lingchao Zhang, [a] Jinmei Bao, [a] Pengyan Gao, [a] Qiaochuan Chen *[c], and Qingquan He *[d]

[a]School of Environmental and Chemical Engineering, Shanghai University, Shanghai 200444, China

[b]School of Chemistry and Chemical Engineering, Qiannan Normal University for Nationalities, Duyun 558000, China

[c]School of Computer Engineering and Science, Shanghai Univerisity, Shanghai, China

[d]College of Materials Science and Engineering, Zhejiang University of Technology, Hangzhou 310014, China

*Corresponding authors:

K. Peng (pkmchem@sgmtu.edu.cn); Q. Chen, (qcchen@shu.edu.cn); Q. He (qqhe21@zjut.edu.cn);

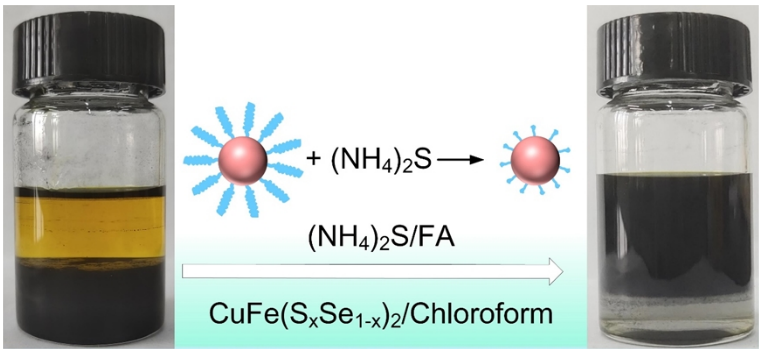

Fig. S1. Black colored colloidal dispersion of $CuFe(S_xSe_{1-x})_2$ NPs undergoes the phase transfer from chloroform to formamide (FA) upon exchange of the original organic surface ligands with S^{2-}.

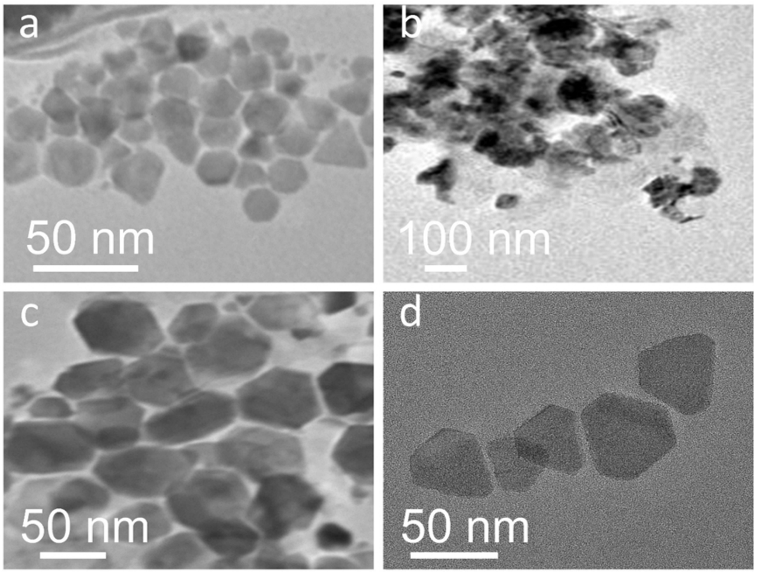

Fig. S2. TEM images of (a) $CuFeSe_2$, (b) $CuFe(S_{0.45}Se_{0.55})_2$, (c) $CuFe(S_{0.63}Se_{0.37})_2$, and (d) $CuFeS_2$.

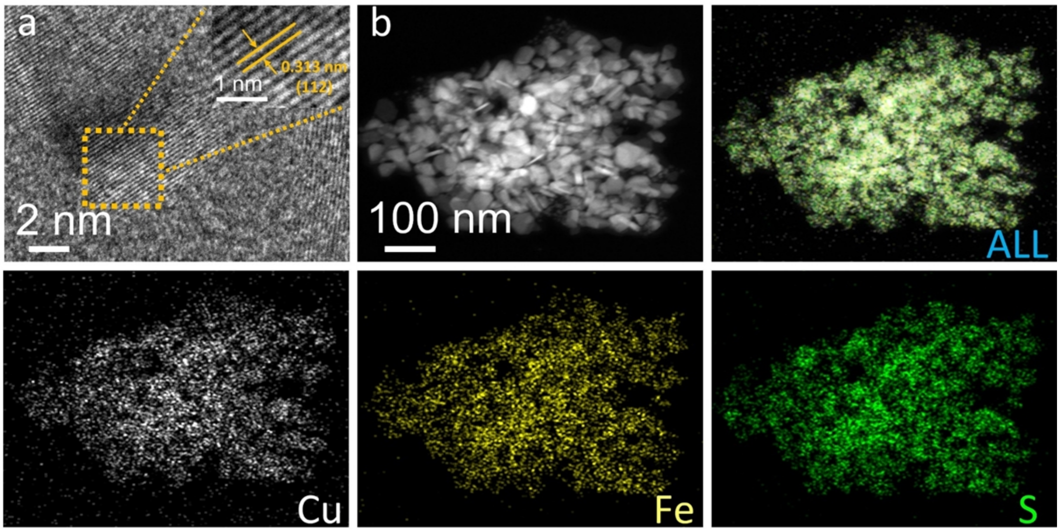

Fig. S3. HRTEM images (a) and EDS mapping images (b) of the $CuFeS_2$ samples.

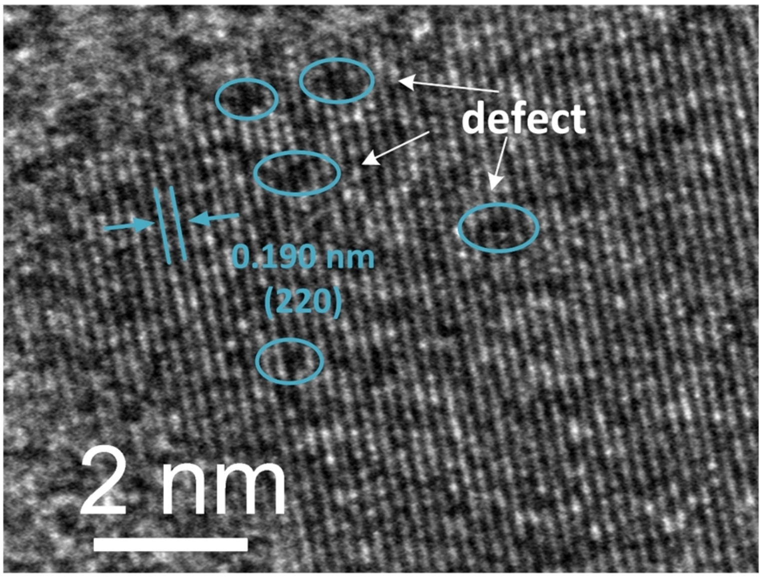

Fig. S4. The typical HRTEM image of a nanoplate derived from the as-synthesized $CuFe(S_{0.8}Se_{0.2})_2$ catalyst.

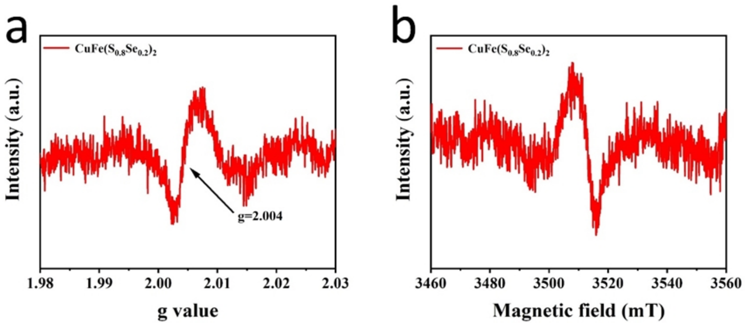

Fig. S5. EPR spectrum of the as-synthesized $CuFe(S_{0.8}Se_{0.2})_2$ samples.

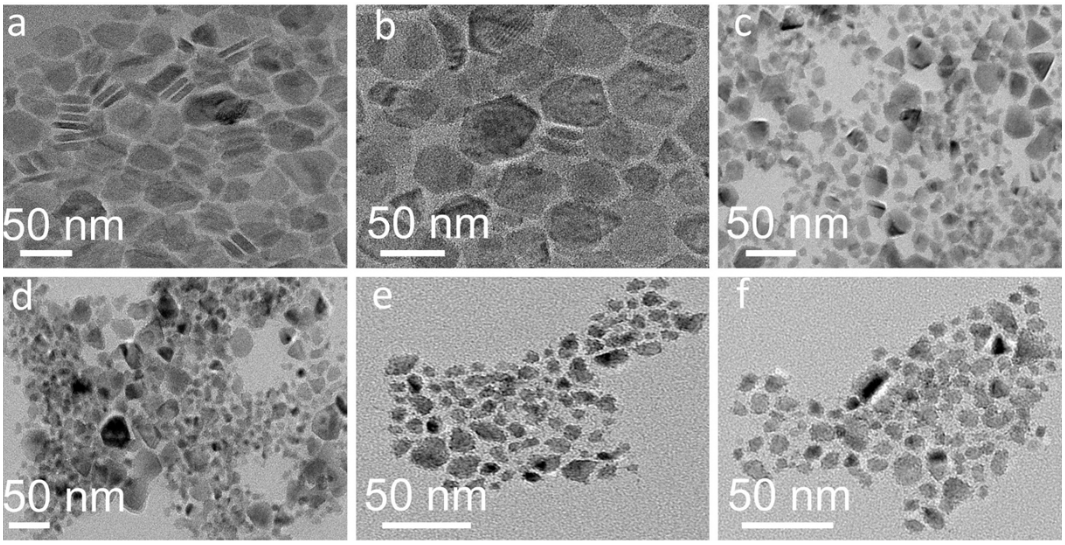

Fig. S6. TEM images of $CuFe(S_{0.8}Se_{0.2})_2$ at different temperatures (a-b) 90 ℃, (c-d) 135 ℃, and (e-f) 180℃.

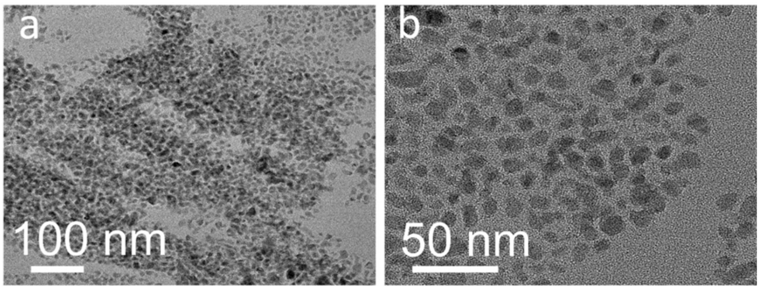

Fig. S7. TEM image of $CuFe(S_{0.8}Se_{0.2})_2$ synthesized by 1-DDT instead of t-DDT.

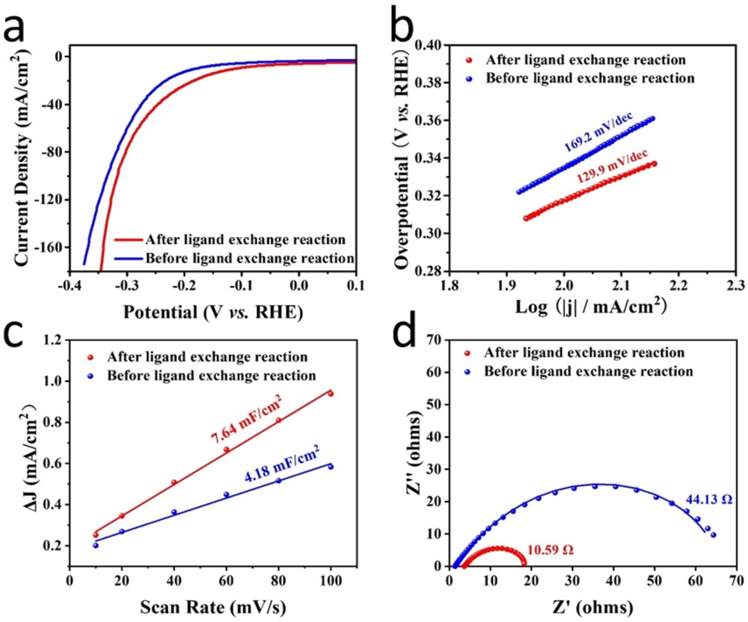

Fig. S8. HER performance in 1 M KOH solution. (a) LSV curves, (b) the Tafel plots, (c) the fitted C_{dl} and (d) Nyquist plots of the $CuFe(S_{0.8}Se_{0.2})_2$ samples before/after ligand exchange reaction.

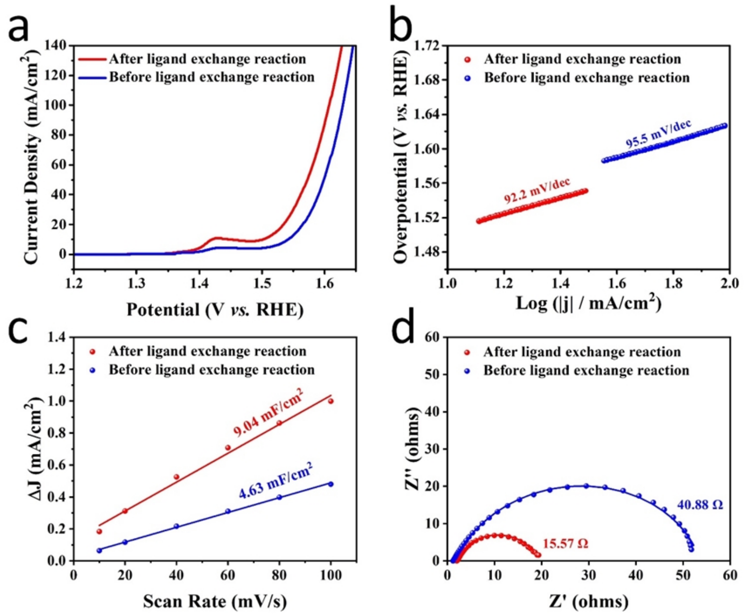

Fig. S9. OER performance in 1 M KOH solution. (a) LSV curves, (b) the Tafel plots, (c) the fitted C_{dl} and (d) Nyquist plots of the $CuFe(S_{0.8}Se_{0.2})_2$ samples before/after ligand exchange reaction.

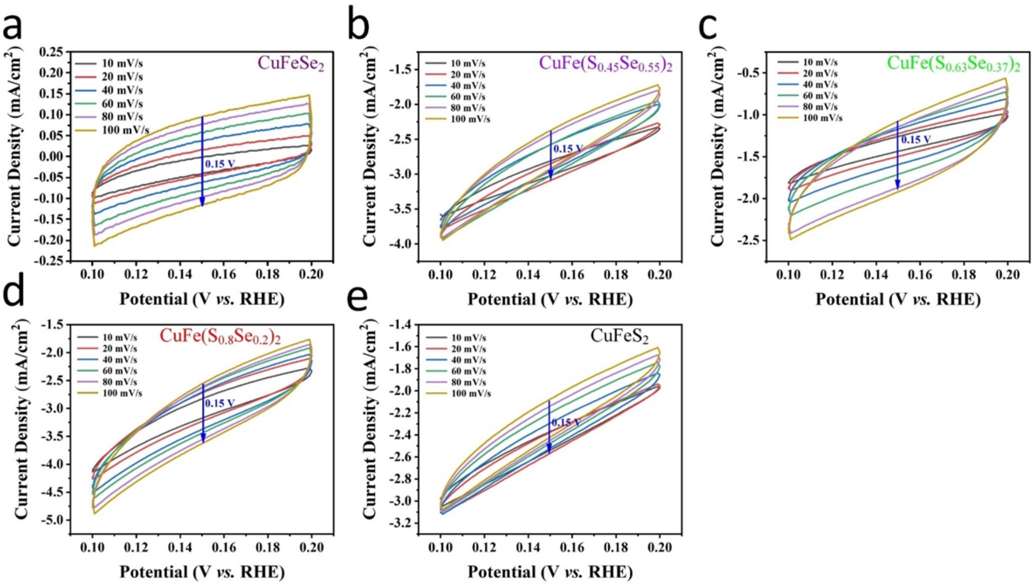

Fig. S10. CV curves of (a) $CuFeSe_2$, (b) $CuFe(S_{0.45}Se_{0.55})_2$, (c) $CuFe(S_{0.63}Se_{0.37})_2$, (d) $CuFe(S_{0.8}Se_{0.2})_2$ and (e) $CuFeS_2$ at different scan rates from 10 to 100 mV/s towards HER in 1.0 M KOH.

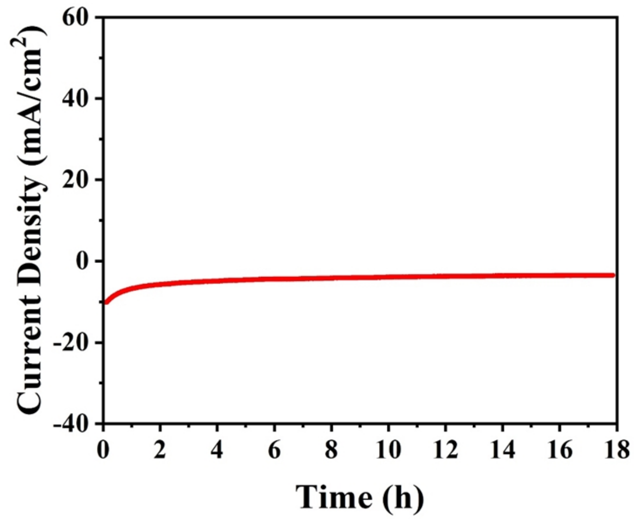

Fig. S11. The long stability tests of the $CuFe(S_{0.8}Se_{0.2})_2$ catalysts in 1 M KOH.

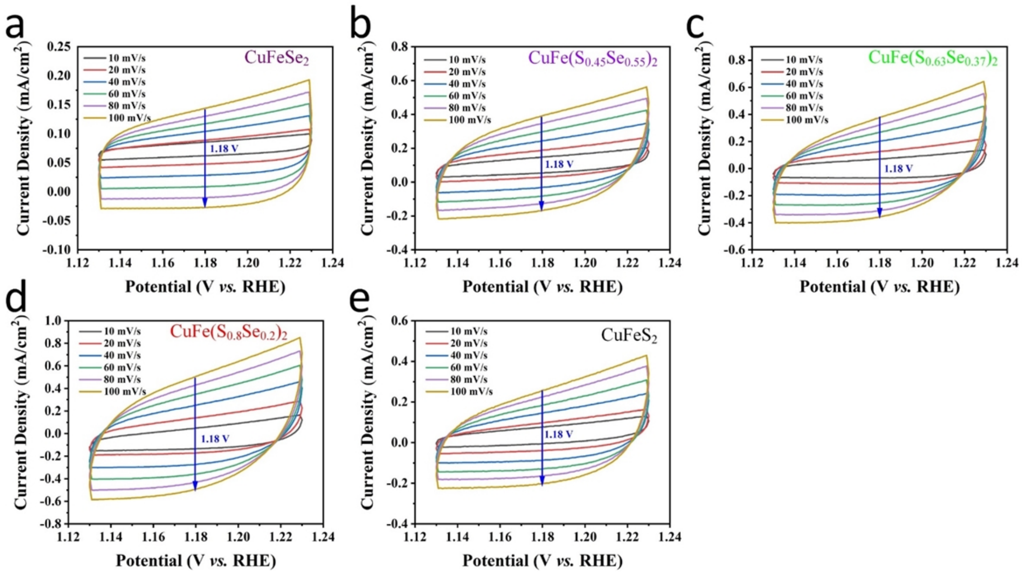

Fig. S12. CV curves of (a) $CuFeSe_2$, (b) $CuFe(S_{0.45}Se_{0.55})_2$, (c) $CuFe(S_{0.63}Se_{0.37})_2$, (d) $CuFe(S_{0.8}Se_{0.2})_2$ and (e) $CuFeS_2$ at different scan rates from 10 to 100 mV/s towards OER in 1.0 M KOH.

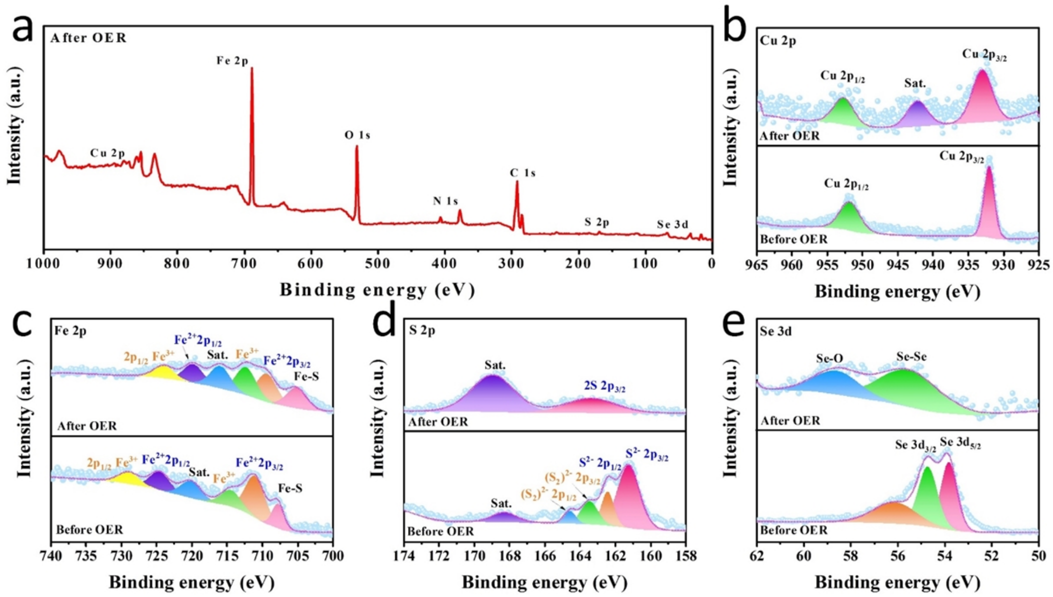

Fig. S13. XPS spectra for (a) survey, (b) Cu 2p, (c) Fe 2p, (d) S 2p, and (e) Se 3d of $CuFe(S_{0.8}Se_{0.2})_2$ before and after OER stability test.

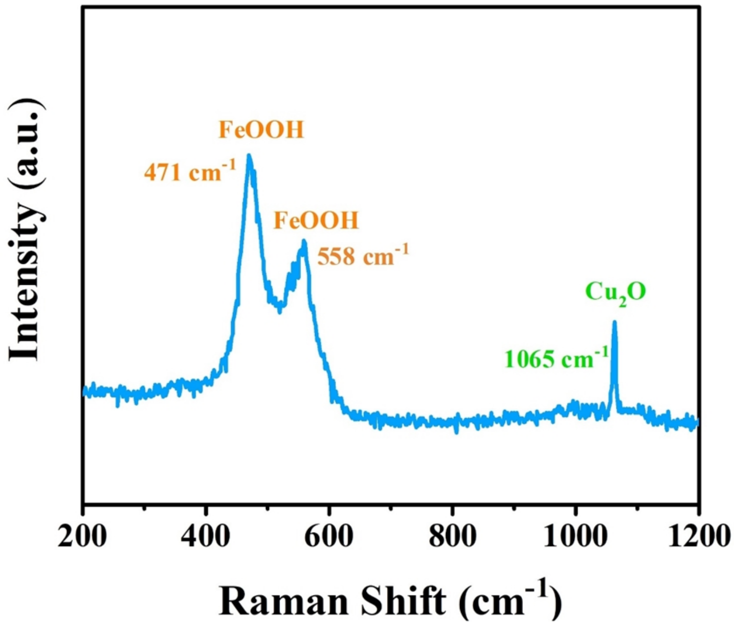

Fig. S14. Raman spectra of the $CuFe(S_{0.8}Se_{0.2})_2$ catalysts after OER test.

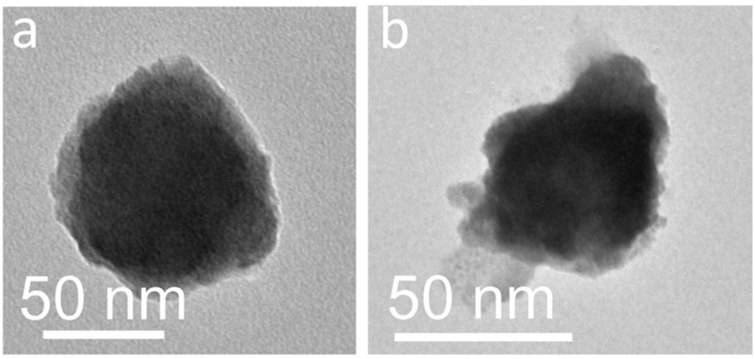

Fig. S15. The TEM images of the $CuFe(S_{0.8}Se_{0.2})_2$ catalysts after OER test.

Table S1

EDX results for $CuFe(S_xSe_{1-x})_2$ catalysts.

Catalysts	**Cu:Fe:S:Se actom ratio from EDS**
$CuFeSe_2$	31.99 : 19.37 : 48.64
$CuFe(S_{0.45}Se_{0.55})_2$	25.24 : 22.16 : 23.78 : 28.82
$CuFe(S_{0.63}Se_{0.37})_2$	27.06 : 20.55 : 33.15 : 19.24
$CuFe(S_{0.8}Se_{0.2})_2$	34.62 : 17.69 : 38.28 : 9.41
$CuFeS_2$	27.93 : 20.63 : 51.44

Table S2

ICP results for $CuFe(S_{0.8}Se_{0.2})_2$ catalysts.

Catalysts	**Cu:Fe:S:Se ratio from ICP**
$CuFe(S_{0.8}Se_{0.2})_2$	28.27 : 28.34 : 34.9 : 8.49

Table S3

Equivalent circuit fitting parameters for the $CuFe(S_xSe_{1-x})_2$ catalysts.

electrolyte	Catalysts	R_s (Ω)	R_{ct} (Ω)
1 M KOH (HER)	$CuFeSe_2$	1.89	304.4
	$CuFe(S_{0.45}Se_{0.55})_2$	1.161	104
	$CuFe(S_{0.63}Se_{0.37})_2$	2.345	27.41
	$CuFe(S_{0.8}Se_{0.2})_2$	3.667	10.59
	$CuFeS_2$	2.167	213.4
1 M KOH (OER)	$CuFeSe_2$	2.916	192.8
	$CuFe(S_{0.45}Se_{0.55})_2$	1.585	78.41
	$CuFe(S_{0.63}Se_{0.37})_2$	2.295	28.53
	$CuFe(S_{0.8}Se_{0.2})_2$	1.843	15.57
	$CuFeS_2$	1.709	145.3

Table S4

The OER activity of the $CuFe(S_{0.8}Se_{0.2})_2$ catalyst in this work. Comparison with recently reported transition metal-based chalcogenides electrocatalysts.

Catalyst	Electrode	Electrolyte	Overpotential (mV) at 10 mA/cm^2	References
$MoSe_2$–Cu_2S	GCE	1 M KOH	264	[1]
MoS_2/NiS_2-3	CC	1 M KOH	278	[2]
CuSe	NF	1 M KOH	297	[3]
CuFe/NF	NF	1 M KOH	218	[4]
Cu@CoFe LDH	CF	1 M KOH	240	[5]
NiS_2/MoS_2-2	CC	1 M KOH	270	[6]
$CuFeS_2$	NF	1 M KOH	320	[7]
Co-Fe(1/1)-Se	GCE	1 M KOH	270	[8]
$CoFe_{0.7}Se_{1.7}$	CP	1 M KOH	279	[9]
$Fe_7S_8/FeS_2/C$	NF	1 M KOH	262	[10]
$CuFe(S_{0.8}Se_{0.2})_2$	NF	1 M KOH	271	This work

NF: Ni foam; GCE: glassy carbon electrode; CF: Cu foam;

Table S5

The OWS activity of the $CuFe(S_{0.8}Se_{0.2})_2$ catalyst in this work. Comparison with recently reported transition metal-based chalcogenides electrocatalysts.

Catalyst	Electrode	Electrolyte	Overpotential (mV) at 10 mA/cm^2	References
MoS_2/NiS_2-3	CC	1 M KOH	1.59	[2]
CuSe	NF	1 M KOH	1,68	[3]
CuFe/NF	NF	1 M KOH	1.64	[4]
Cu@CoFe LDH	Cu foam	1 M KOH	1.68	[5]
$CuFeS_2$	NF	1 M KOH	1.66	[7]
Co-Fe(1/1)-Se	GCE	1 M KOH	1.68	[8]
$Fe_7S_8/FeS_2/C$	NF	1 M KOH	1.67	[10]
Co_9S_8-Ni_3S_2-CNTs/NF	NF	1 M KOH	1.65	[11]
EG/$Co_{0.85}$Se/NiFeLDH	EG	1 M KOH	1.67	[12]
Fe-doped NiS–NiS_2	NF	1 M KOH	1.59	[13]
$CuFe(S_{0.8}Se_{0.2})_2$	NF	1 M KOH	1.61	This work

NF: Ni foam; GCE: glassy carbon electrode; CF: Cu foam;

References

1. M. S. Hassan, P. Basera, S. Gahlawat, P. P. Ingole, S. Bhattacharya and S. Sapra, Understanding the efficient electrocatalytic activities of $MoSe_2$–Cu_2S nanoheterostructures, *J. Mater. Chem. A*, 2021, **9**, 9837-9848.
2. J. H. Lin, P. C. Wang, H. H. Wang, C. Li, X. Q. Si, J. L. Qi, J. Cao, Z. X. Zhong, W. D. Fei and J. C. Feng, Defect-Rich Heterogeneous MoS_2/NiS_2 Nanosheets Electrocatalysts for Efficient Overall Water Splitting, *Adv. Sci.*, 2019, **6**, 1900246.
3. B. Chakraborty, R. Beltran-Suito, V. Hlukhyy, J. Schmidt, P. W. Menezes and M. Driess, Crystalline Copper Selenide as a Reliable Non-Noble Electro(pre)catalyst for Overall Water Splitting, *Chemsuschem*, 2020, **13**, 3222-3229.
4. A. I. Inamdar, H. S. Chavan, B. Hou, C. H. Lee, S. U. Lee, S. Cha, H. Kim and H. Im, A Robust Nonprecious CuFe Composite as a Highly Efficient Bifunctional Catalyst for Overall Electrochemical Water Splitting, *Small*, 2020, **16**, e1905884.
5. L. Yu, H. Q. Zhou, J. Y. Sun, F. Qin, D. Luo, L. X. Xie, F. Yu, J. M. Bao, Y. Li, Y. Yu, S. Chen and Z. F. Ren, Hierarchical Cu@CoFe layered double hydroxide core-shell nanoarchitectures as bifunctional electrocatalysts for efficient overall water splitting, *Nano Energy*, 2017, **41**, 327-336.
6. Y. Qian, J. Yu, Y. Zhang, F. Zhang, Y. Kang, C. Su, H. Shi, D. J. Kang and H. Pang, Interfacial Microenvironment Modulation Enhancing Catalytic Kinetics of Binary Metal Sulfides Heterostructures for Advanced Water Splitting Electrocatalysts, *Small Methods*, 2022, **6**, 2101186.
7. A. Sathyaseelan, D. Kesavan, S. Manoharan, V. K. Mariappan, K. Krishnamoorthy and S. J. Kim, Thermoelectric Driven Self-Powered Water Electrolyzer Using Nanostructured $CuFeS_2$ Plates as Bifunctional Electrocatalyst, *ACS Appl. Energy Mater.*, 2021, **4**, 7020-7029.
8. F. O. Boakye, Y. Li, K. A. Owusu, I. S. Amiinu, Y. P. Cheng and H. N. Zhang, One-step synthesis of heterostructured cobalt-iron selenide as bifunctional catalyst for overall water splitting, *Mater. Chem. Phys.*, 2022, **275**, 125201.
9. X. Y. Wang, Y. Zhou, M. Liu, C. Chen and J. Zhang, Colloidal synthesis of high-performance FeSe/CoSe nanocomposites for electrochemical oxygen evolution reaction, *Electrochim. Acta.*, 2019, **297**, 197-205.

10. Y. Xu, T. T. Feng, Z. J. Cui, P. F. Guo, W. P. Wang and Z. C. Li, $Fe_7S_8/FeS_2/C$ as an efficient catalyst for electrocatalytic water splitting, *Int. J. Hydrogen Energy*, 2021, **46**, 39216-39225.

11. Y. Yao, J. He, L. Ma, J. Wang, L. Peng, X. Zhu, K. Li and M. Qu, Self-supported Co_9S_8-Ni_3S_2-CNTs/NF electrode with superwetting multistage micro-nano structure for efficient bifunctional overall water splitting, *J. Colloid. Interf. Sci.*, 2022, **616**, 287-297.

12. Y. Hou, M. R. Lohe, J. Zhang, S. H. Liu, X. D. Zhuang and X. L. Feng, Vertically oriented cobalt selenide/NiFe layered-double-hydroxide nanosheets supported on exfoliated graphene foil: an efficient 3D electrode for overall water splitting, *Energy Environ. Sci.*, 2016, **9**, 478-483.

13. S. S. Huang, Q. Zhang, P. J. Xin, J. Zhang, Q. C. Chen, J. Fu, Z. Q. Jin, Q. Wang and Z. J. Hu, Construction of Fe-doped NiS-NiS_2 Heterostructured Microspheres Via Etching Prussian Blue Analogues for Efficient Water-Urea Splitting, *Small*, 2022, e2106841.